RADIO–TO–FAR-INFRARED SPECTRAL ENERGY DISTRIBUTION AND PHOTOMETRIC REDSHIFTS FOR DUSTY STARBURST GALAXIES

MIN S. YUN

University of Massachusetts, Department of Astronomy, Amherst, MA 01003; myun@astro.umass.edu

AND

C. L. CARILLI

National Radio Astronomy Observatory, P.O. Box O, Socorro, NM 87801; ccarilli@nrao.edu

ABSTRACT

As a logical next step in improving the radio-to-submillimeter spectral index as a redshift indicator, we have investigated a technique of using the entire radio–to–far-infrared spectral energy distribution (SED) for deriving photometric redshifts for dusty starburst galaxies at high redshift. A dusty starburst SED template is developed from the theoretical understanding of various emission mechanisms related to massive star formation processes, and the template parameters are selected by examining the observed properties of 23 IR-selected starburst galaxies: $T_d = 58$ K, $\beta = 1.35$, and $f_{nth} = 1$. The major improvement in using this template SED for deriving photometric redshifts is the significant reduction in redshift uncertainty over the spectral index technique, particularly at higher redshifts. Intrinsic dispersion in the radio and far-infrared SEDs as well as absolute calibration and measurement errors contribute to the overall uncertainty of the technique. The derived photometric redshifts for five submillimeter galaxies with known redshifts agree well with their spectroscopic redshifts within the estimated uncertainty. Photometric redshifts for seven submillimeter galaxies without known spectroscopic redshifts (HDF 850.1, CUDSS 14.1, Lockman 850.1, SMM J00266+1708, SMM J09429+4658, SMM J14009+0252, and FIRBACK J1608+5418) are derived.

Subject heading: galaxies: high-redshift — galaxies: starburst — infrared: galaxies — radio continuum: galaxies — submillimeter — techniques: photometric

1. INTRODUCTION

Sensitive observations at submillimeter wavelengths are revealing what may be a population of active star-forming galaxies at high redshift that are unseen in deep optical surveys because of dust obscuration (Smail, Ivison, & Blain 1997; Barger et al. 1998; Hughes et al. 1998; Eales et al. 1999). The differential source counts clearly indicate a large excess of far-infrared (FIR) sources by a factor of 10–50 over the no-evolution models derived from the optical deep survey data (Guiderdoni et al. 1998; Blain et al. 1999; Matsuhara et al. 2000; Scott et al. 2002), and a large fraction of star formation may be hidden by dust. The analysis of the submillimeter SCUBA source counts and inferred redshift distribution based on the radio-submillimeter flux density ratio (Carilli & Yun 1999) suggests that luminous dusty galaxies may dominate star formation history at early epochs ($z \sim 1$–3; Barger, Cowie, & Richards 2000). Many of these faint submillimeter sources are found to be very faint, red ($R \geq 25$, $K \geq 21$) sources (Smail et al. 1999), whose optical redshifts may be inaccessible even for the 10 m class telescopes. These galaxies are nearly entirely missing from the optical studies of star formation at high redshifts (e.g., Steidel et al. 1999; Chapman et al. 2000), and a significant revision to the optically derived cosmic star formation history may be needed (see Blain et al. 1999).

Because direct redshift measurements are not possible in most cases, the redshift distribution and the cosmic evolution of the dusty submillimeter galaxy population are not well determined at the moment. In a recent paper, we have proposed a technique of using the radio-to-submillimeter spectral index as a redshift indicator. This technique is based on the universal radio-to-FIR correlation for star-forming galaxies (Condon 1992), with the assumption that the spectral shapes may be similar enough to be able to differentiate between low- and high-redshift objects (see Carilli & Yun 1999). To understand the magnitude of scatter in this relation and resulting uncertainty in the redshift estimates, we derived an empirical $\alpha_{1.4}^{350}$-z relation[1] using the observed spectral energy distributions (SEDs) of 17 low-redshift starburst galaxies (Carilli & Yun 2000; also see Dunne, Clements, & Eales 2000a). There is significant scatter, but the existing data on high-redshift star-forming galaxies and active galactic nucleus (AGN) hosts appear to follow this relation well.

While the radio-to-submillimeter spectral index has been demonstrated to be a useful redshift indicator, using it to derive a redshift for any particular object may be risky because of the scatter in the observed $\alpha_{1.4}^{350}$-z relation and the flattening in the relation at high redshifts. Obtaining redshift estimates using flux density ratios at other wavelength bands has also been suggested, although none is particularly more successful (e.g., Hughes et al. 1998; Blain 1999; Hines & Low 1999; Fox et al. 2002). More accurate redshift estimates for dusty starburst galaxies may be obtained by utilizing the information associated with the *entire radio-to-FIR SED*. Such a photometric redshift technique requires a good SED template, and here we derive an SED template based on the theoretical expectations of thermal dust, thermal bremsstrahlung, and nonthermal synchrotron emission from a dusty starburst galaxy. Our SED template is constructed by examining the properties of the 23 IR-selected

---

[1] The term $\alpha_{1.4}^{350}$ is the spectral index between 1.4 and 350 GHz.

starburst galaxies whose submillimeter/FIR SED data are readily available in the literature. When applied to a sample of submillimeter galaxies with known redshifts, the resulting redshift estimates are in excellent agreement with the spectroscopic redshifts. We also report photometric redshifts for a sample of submillimeter galaxies without known spectroscopic redshifts, including the brightest SCUBA source in the Hubble Deep Field (Hughes et al. 1998).

2. STARBURST SPECTRAL ENERGY DISTRIBUTION MODEL

The observed SED from radio-to-infrared wavelengths for a dusty starburst galaxy is dominated by the energetic signatures of young stars and their environment. The bulk of the radiation from young OB stars is absorbed by dust and reemitted in the infrared. The H II regions surrounding the young stars are also the sources of thermal bremsstrahlung (free-free) emission. Energetic electrons produced in supernovae and their remnants are thought to account for nearly all of the radio synchrotron radiation. Following the discussion by Condon (1992), a simple starburst SED model is constructed as a linear sum of dust continuum (S_d), thermal bremsstrahlung or free-free (S_{th}), and nonthermal synchrotron (S_{nth}) emission.

2.1. *Thermal Dust Emission*

The flux density, $S_d(\nu)$, from a cloud at a distance D_L containing N spherical dust grains each of cross section σ_d, temperature T_d, and emissivity $Q(\nu)$ is given by

$$S_d(\nu) = N(\sigma_d/D_L^2)Q(\nu)B(\nu, T_d) , \qquad (1)$$

where $B(\nu, T_d)$ is the Planck function describing thermal blackbody radiation. The term $N(\sigma_d/D_L^2)$ is the solid angle Ω_d subtended by the dust source in the sky. For the emissivity function, we adopt a form

$$Q(\nu) = 1 - \exp\left[-\left(\frac{\nu}{\nu_c}\right)^\beta\right], \qquad (2)$$

where β is the dust emissivity index generally thought to be between 0 and 2 (Hildebrand 1983). This particular functional form allows the dust spectrum to be that of a purely blackbody above the critical frequency ν_c where the dust clouds become optically thick, while it is that of the $\nu^{2+\beta}$ graybody spectrum at lower frequencies. Observations suggest that thermal dust emission is nearly optically thick even at $\lambda \sim 100$ μm for galaxies dominated by intense starburst regions (see Scoville et al. 1991; Solomon et al. 1997), and we adopt $\nu_c = 2 \times 10^{12}$ Hz ($\lambda_c = 150$ μm). Combining equations (1) and (2),

$$S_d(\nu) = \Omega_d B(\nu, T_d)\left[1 - e^{-(\nu/\nu_c)^\beta}\right] . \qquad (3)$$

For a dust source of θ arcsec in diameter, expected flux density at ν (in gigahertz) due to thermal dust emission is

$$S_d(\nu) = 2.8 \times 10^{-8} \frac{\nu^3\theta^2}{e^{(0.048\nu/T_d)} - 1}\left[1 - e^{-(\nu/2000)^\beta}\right] \text{ Jy} . \qquad (4)$$

The FIR luminosity, L_{FIR}, is derived by integrating equation (4) over the emitting area Ω_d and over the frequency range corresponding to $\lambda = 40$–500 μm,

$L_{FIR} = 4\pi D_L^2 \int \int S_d(\nu)d\nu\, d\Omega$. The massive star formation rate (SFR) for a dusty starburst galaxy is then directly related to its dust continuum spectrum by the FIR luminosity (i.e., SFR $= L_{FIR}/(5.8 \times 10^9 L_\odot)$ $M_\odot$ yr^{-1}; Kennicutt 1998).

2.2. *Thermal Bremsstrahlung (Free-Free) Emission*

Thermal bremsstrahlung (free-free) emission from ionized gas in the H II regions surrounding hot young stars can be described in the same functional form as the thermal dust emission as in equation (3),

$$S_{ff}(\nu) = \Omega_{ff}B(\nu, T_e)(1 - e^{-\tau_{ff}}) , \qquad (5)$$

where T_e is electron temperature and τ_{ff} is free-free optical depth at the observed frequency. In the Rayleigh-Jeans regime ($h\nu \ll kT$), $B(\nu, T_e) = 2kT_e\nu^2/c^2$ at radio frequencies, and

$$S_{ff}(\nu) = 2kT_e\nu^2 c^{-2}\Omega_{ff}(1 - e^{-\tau_{ff}}) . \qquad (6)$$

Free-free optical depth is given by $\tau_{ff} = 0.083EM\nu^{-2.1}T_e^{-1.35}$, where $EM \equiv \int n_e^2\, dl$ (cm^{-6} pc) is the emission measure. In the optically thin regime, thermal bremsstrahlung emission then has the familiar $\nu^{-0.1}$ dependence. A circular source of θ arcsec in diameter would have a flux density of

$$S_{ff}(\nu) = 4.8 \times 10^{-8}EM\nu^{-0.1}T_e^{-0.35}\theta^2 \text{ Jy} . \qquad (7)$$

2.3. *Nonthermal Synchrotron Emission*

For an ensemble of relativistic electrons with a power-law distribution of energy $N(E) = N_0 E^{-\gamma}$ and an isotropic velocity distribution, their synchrotron emission coefficient is

$$\epsilon \propto N_0(B\sin\theta)^{(\gamma+1)/2}\nu^{(1-\gamma)/2} , \qquad (8)$$

where θ is the angle between the magnetic field B and the line of sight to the observer. The resulting power-law spectrum has a form $S_\nu \propto \nu^{-\alpha}$, where $\alpha = (\gamma - 1)/2$ is the spectral index. Bell (1978) proposed the acceleration of cosmic rays by supersonic shocks (of velocity v_s) as the main mechanism for nonthermal synchrotron emission from supernova remnants and derived the volume emissivity as

$$\epsilon(\nu) \sim 3 \times 10^{-33}\nu^{-\alpha}\frac{n}{\text{cm}^{-3}}\frac{\alpha}{0.75}$$
$$\times \left(\frac{v_s}{10^4 \text{ km s}^{-1}}\right)^{4\alpha}\left(\frac{B}{10^{-4} \text{ G}}\right)^{\alpha+1} \text{ ergs s}^{-1} \text{ Hz}^{-1} \text{ cm}^{-3}. \qquad (9)$$

Assuming supernova remnants dominate the nonthermal synchrotron emission from galaxies, Condon (1992) derived a relation $S_{nth} \propto \nu_{SN}$, where ν_{SN} is the Type II supernova rate per year (see his eq. [17]). However, this relation predicts a ν_{SN} more than an order of magnitude too large for our Galaxy, and Condon proposed a revised relation based on Galactic normalization (i.e., his eq. [18]), which can be rewritten as

$$S_{nth}(\nu) = 1150\nu^{-\alpha}\nu_{SN}D_L^{-2} \text{ Jy} , \qquad (10)$$

where D_L is luminosity distance in megaparsecs.

TABLE 1
SPECTRAL ENERGY DISTRIBUTION MODEL FITS

Name	L_{FIR} ($\times 10^{10}\ L_\odot$)	SFR[a] ($M_\odot$ yr^{-1})	T_d (K)	β[b]	f_{nth}[c]	"z_{ph}"
Zw 049.057..............	10	18	54	1.30	0.6	+0.06
NGC 5256................	11	19	51	1.35	4.0	+0.07
MCG +00-29-023	11	19	49	1.15	1.3	+0.25
NGC 3110................	12	20	46	1.35	1.2	+0.19
Mrk 331	16	27	57	1.15	0.8	+0.06
NGC 1614................	21	37	61	1.40	1.0	−0.07
UGC 2369................	21	37	52	1.30	1.2	+0.16
NGC 2623................	21	37	57	1.45	1.1	−0.07
Arp 193	25	42	47	1.70	1.5	+0.01
Arp 148	25	42	50	1.20	0.9	+0.22
IRAS 10173+0828 ...	33	57	69	1.10	0.6	+0.02
NGC 6240................	35	61	49	1.45	3.9	−0.07
Mrk 848	35	61	62	1.20	1.6	+0.06
IRAS 15250+3609 ...	48	82	74	1.05	1.1	+0.01
UGC 5101................	54	93	47	1.40	2.5	+0.14
IRAS 08572+3915 ...	55	93	74	1.60	0.3	−0.22
IRAS 05189−2524	57	98	70	1.05	0.6	+0.05
IRAS 10565+24	60	104	55	1.55	0.4	+0.06
Mrk 273	73	127	61	1.40	1.7	−0.10
Arp 220	95	163	59	1.15	1.0	+0.05
IRAS 12112+0305 ...	106	183	63	1.25	0.8	+0.02
IRAS 14348−1447	109	187	63	1.50	1.0	+0.09
Mrk 231	137	236	72	1.35	2.0	−0.30

[a] SFR = $L_{\text{FIR}}/(5.8 \times 10^9\ L_\odot)\ M_\odot$ yr^{-1} (Kennicutt 1998).
[b] Dust emissivity.
[c] Multiplicative correction factor for nonthermal radio continuum emission. The $f_{\text{nth}} = 1.0$ corresponds to the Galactic normalization adopted by Condon 1992.

2.4. Starburst SED Template

The first and the foremost important step in all photometric redshift techniques is establishing a robust and reliable template. Key SED template parameters for the starburst SED template are T_d and β for the dust emission (eq. [4]), T_e and EM for thermal free-free emission (eq. [7]), and ν_{SN} and α for the nonthermal synchrotron emission (eq. [10]). These parameters and their dispersions are determined by deriving best-fit SED models for the 23 IR-selected starburst galaxies whose submillimeter/FIR data are readily available in the literature.

Flux density for dust emission S_d can be derived directly using equation (3) by specifying the source size Ω_d, dust temperature T_d, and emissivity β. The effective source solid angle Ω_d for a given source is derived from the observed 100 μm flux density, assuming dust emission is nearly optically thick (see § 2.1). For example, the prototypical ultraluminous galaxy Arp 220 is a 114 Jy (1.14×10^{-21} ergs cm^{-2} Hz^{-1}) source at 100 μm, which translates to $\Omega_d = 3 \times 10^{-11}$ rad^2 for $T_d = 59$ K (see Table 1). This corresponds to a circular area with 1″.2 (390 pc) in diameter,[2] which agrees well with the size of the molecular gas complex fueling the nuclear starburst traced in CO (Scoville, Yun, & Bryant 1997; Downes & Solomon 1998; Sakamoto et al. 1999). The best-fit dust SED model is then selected by examining the parameter space for T_d and β, between 25 and 85 K and 1.0 and 2.0, respectively.

Thermal bremsstrahlung or free-free flux densities can be derived from equation (7) by determining the frequency where free-free opacity τ_{ff} becomes unity and estimating the size of the emitting region. Alternatively, one can also compute the free-free flux density from the inferred SFR as it is proportional to the production rate of Lyman continuum photons. Using the Hα normalization of Kennicutt (1998) for a Salpeter initial mass function and assuming that 50% of Lyman continuum photons are quenched by dust absorption, equation (23) of Condon (1992) can be rewritten as

$$L_{\text{ff}}(\nu) = 7.9 \times 10^{26} \nu^{-0.1} \frac{\text{SFR}}{M_\odot\ \text{yr}^{-1}}\ \text{ergs s}^{-1}\ \text{Hz}^{-1}\ . \quad (11)$$

The free-free flux density for a galaxy with a given FIR-derived star formation rate is then

$$S_{\text{ff}}(\nu) = 0.71 \nu^{-0.1} \frac{\text{SFR}}{M_\odot\ \text{yr}^{-1}} D_L^{-2}\ \text{Jy}\ . \quad (12)$$

The free-free flux density S_{ff} determined this way is nearly identical to the value derived using equation (7) assuming $\tau_{\text{ff}} \sim 1$ at $\nu = 1$ GHz and $\Omega_{\text{ff}} = \Omega_d$.

Nonthermal synchrotron flux density S_{nth} can also be parameterized as a function of SFR since $\nu_{\text{SN}} \propto$ SFR. Adjusting equation (20) of Condon (1992) for the Salpeter initial mass function, equation (10) can be rewritten as

$$S_{\text{nth}}(\nu) = 25 f_{\text{nth}} \nu^{-\alpha} \frac{\text{SFR}}{M_\odot\ \text{yr}^{-1}} D_L^{-2}\ \text{Jy}\ . \quad (13)$$

The synchrotron spectral index α is known to lie within a narrow range around 0.7–0.8, and we simply adopt $\alpha = 0.75$ to minimize the number of free parameters in our

---

[2] An ensemble of distributed sources with the equivalent total area is also allowed by this simple model.
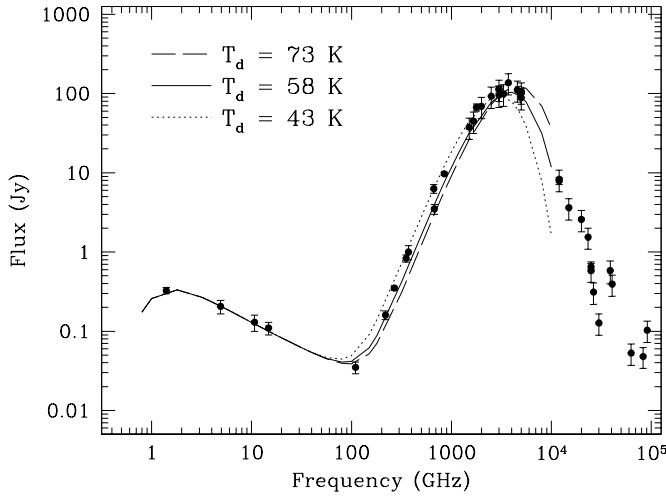
FIG. 1.—Radio-to-IR SED for Arp 220 is shown along with the model starburst SEDs with $\beta = 1.35$ and $T_d = 43$, 58, and 73 K. The radio-FIR normalization term f_{nth} is set to 1.0, which is the Galactic normalization by Condon (1992).

FIG. 2.—Distribution of best-fit β values vs. T_d for the 23 luminous IR starburst galaxies. The median values for β and T_d are 1.35 and 57 K, while the mean values are 1.32 ± 0.17 and 58 ± 9 K, respectively.

model. Condon's original derivation arbitrarily employed a Galactic normalization as noted earlier. We thus add a scaling factor f_{nth} (of order unity) here in order to determine the normalization more suitable for starburst galaxies.

Only the SED data at frequencies near and below the dust peak are used for the model fit because the mid- to near-IR data points clearly require additional, higher temperature dust components.

The SED fit for Arp 220 is shown in Figure 1, and it demonstrates the effects of changing T_d while holding β constant. The scatter of data points about various models suggests that there are systematic scaling differences among different flux density measurements, generally larger than the nominal uncertainties reported, especially in the submillimeter wavelengths. At a glance, all three dust temperature models plotted seem to do an adequate job of fitting the submillimeter and FIR data points qualitatively. However, a closer examination reveals that the $T_d = 74$ K model fails to match the submillimeter points. The $T_d = 43$ K model matches the submillimeter data points reasonably well, but it clearly falls short on predicting the FIR data points. Previous studies of submillimeter dust properties for luminous infrared galaxies generally favored cold dust temperature between 40 and 50 K for Arp 220 (e.g., Eales, Wynn-Williams, & Duncan 1989; Scoville et al. 1991; Dunne et al. 2000b). If we were to choose a *single-temperature* dust SED model that best fits all observed data points between 1 mm and 60 μm, however, a slightly warmer dust model would be favored.

Our starburst SED model analysis is applied to 23 IR-selected starburst galaxies that are selected for (1) their L_{FIR} exceeding $10^{11} L_\odot$ and (2) having at least two measurements covering their submillimeter part of the spectrum. The SED data are primarily drawn from the *IRAS* Faint Source Catalog, the NRAO/VLA Sky Survey (Condon et al. 1998), Condon et al. (1991), Carico et al. (1992), Rigopoulou, Lawrence, & Rowan-Robinson (1996), Benford (1999), Lisenfeld, Isaak, & Hills (2000), Dunne et al. (2000b), and Dunne & Eales (2001). As summarized in Table 1, the characteristic dust temperature T_d ranges between 46 and 74 K, with a mean of 58 ± 9 K. Dust emissivity β also ranges
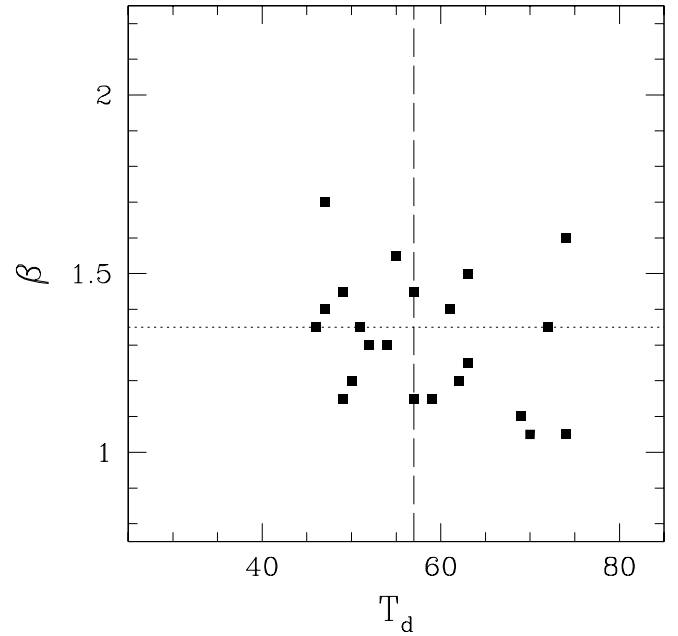
widely, between 1.05 and 1.70, with a mean of 1.32 ± 0.17 and a median of 1.35 (see Fig. 2). It is likely that all galaxies consist of an ensemble of dust clouds with a range of temperature (see Yun & Scoville 1998; Frayer et al. 1999; Dunne & Eales 2001), and single-temperature SED models tend to favor a smaller β (flatter submillimeter dust spectrum) and a higher dust temperature than typically found in giant molecular clouds (10–20 K). Since available SED measurements are generally sparse in practice, we accept these limitations of a single-temperature dust model for the purpose of keeping the number of free parameters manageably small.

Thermal bremsstrahlung (free-free) emission makes significant contribution only in the bottom of the SED trough between the nonthermal synchrotron and thermal dust feature, and it plays essentially no role in defining the starburst SED template. Variations in the nonthermal synchrotron emission are tracked by a parameter f_{nth} (see eq. [13]). The dispersion in the radio-FIR correlation is measured to be about 0.25 in a logarithmic scale (e.g. Yun, Reddy, & Condon 2001), and the rather broad range of f_{nth} found (see Fig. 3) is consistent with this expectation. Presence of a radio AGN (e.g., Mrk 231, NGC 6240) can account for the increase in some cases, but synchrotron emission efficiency may indeed vary from galaxy to galaxy. The median for the whole sample is 1.1, but it is reduced to 1.0 if the two clear radio AGN hosts are removed. Therefore, on average, the nonthermal synchrotron emission from these dusty starburst galaxies appears to follow the Galactic normalization adopted by Condon (1992).

In summary, we adopt $T_d = 58$ K, $\beta = 1.35$, and $f_{nth} = 1.0$ for our photometric redshift SED template. This relatively flat β is in good agreement with the analysis of 102 galaxies by Dunne et al. (2000b), but the mean dust temperature that we adopt is significantly warmer than the mean of $T_d = 36 \pm 5$ K Dunne et al. derived using 60, 100, and 850 μm measurements. The main difference is that the dust emis-
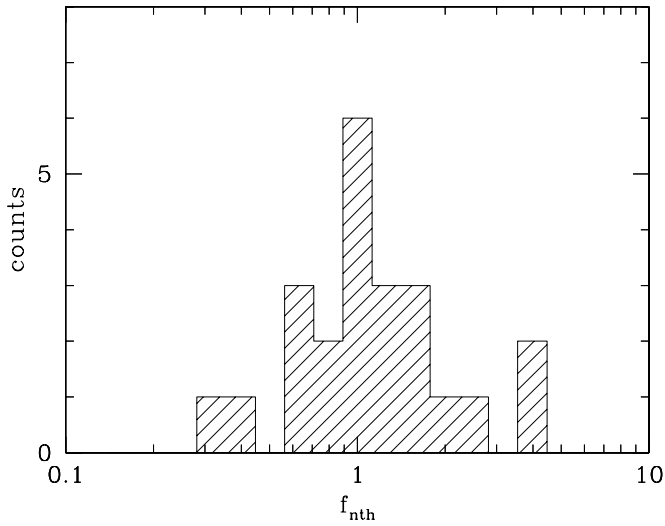
FIG. 3.—Distribution of f_{nth} values for the 23 luminous IR starburst galaxies. The median for the whole sample is 1.1, and it is reduced to 1.0 if two clear radio AGN hosts are removed.

sion from our IR-selected, luminous dusty starburst galaxies are on average significantly warmer than those of the Dunne et al. sample, which includes a large number of late-type field galaxies.

3. PHOTOMETRIC REDSHIFTS FOR DUSTY GALAXIES AT HIGH REDSHIFT

3.1. *Procedure*

Once the dusty starburst SED template is chosen, the entire radio-to-FIR continuum spectrum for any given galaxy can be described in terms of just the total star formation rate SFR and the luminosity distance D_L. The dust spectrum S_d in equation (4) can be rewritten as

$$S_d(\nu) = 1.3 \times 10^{-6} \frac{\text{SFR}(1+z)\nu^3}{D_L^2(e^{0.00083\nu} - 1)} \left[1 - e^{-(\nu/2000)^{1.35}} \right] \text{ Jy} .$$

(14)

Combined with the expressions for free-free and nonthermal synchrotron emission given in equations (12) and (13), the entire radio-to-FIR continuum spectrum can be written as

$$S(\nu_{obs}) = \begin{cases} 25f_{nth}\nu_0^{-\alpha} + 0.71\nu_0^{-0.1} \\ \\ + 1.3 \times 10^{-6} \dfrac{\nu_0^3 \left[1 - e^{-(\nu_0/2000)^{1.35}} \right]}{e^{0.00083\nu_0} - 1} \end{cases} \dfrac{(1+z)\text{SFR}}{D_L^2} \text{ Jy} ,$$

(15)

where SFR is in $M_\odot$ yr^{-1}, D_L in megaparsecs, and $\nu_0 = (1+z)\nu_{obs}$ in gigahertz. A $(1+z)$ term is needed for sources at cosmological distances in order to account for the frequency or wavelength folding by the Doppler effect.

The redshift z and the FIR luminosity (SFR) of a particular galaxy can be determined simultaneously by comparing the observed SED with the dusty starburst template in the (z, SFR) space. To be precise, one needs to include a correc-

tion term accounting for the cosmic microwave background (CMB) because most SED data are measured in contrast to the CMB. In practice, this correction can be safely ignored as long as $T_d/(1+z) \gg 2.7$ K.

As a galaxy is placed further and further away, its entire SED shifts to the bottom (fainter, because of D_L^{-2}) and to the left [lower frequency, $\nu_{obs} = \nu_0/(1+z)$] in the (z, SFR) space. This generic behavior for a dusty starburst galaxy and the resulting change in the apparent spectral index between 1.4 GHz and 850 μm has been pointed out previously as a redshift indicator by Carilli & Yun (1999). The slope of the rising part of the dust spectrum is such that the Doppler shift of the spectrum nearly offsets the D_L^{-2} drop in flux density, making the submillimeter bands particularly attractive for blind searches, but the SED measurements on this part of the dust spectrum offer limited redshift information for the same reason (e.g., Hughes et al. 1998; Fox et al. 2002). As in other photometric redshift techniques, the redshift information comes from distinct spectral features such as the trough between the declining nonthermal synchrotron emission in radio and the sharp rise in the dust spectrum or the dust peak near the rest wavelength of 100 μm. Even when the dust peak in the FIR is not sampled by observations, the radio synchrotron measurements help set the vertical scale with respect to the dust spectrum, i.e., the SFR.

Because SED measurements for most submillimeter galaxies include only a few discrete points rather than a continuous frequency coverage, our best-fit SED model search utilizes a χ^2 minimization with discrete sampling of the parameter space rather than a full cross-correlation technique. One advantage of this approach is that the upper limits in flux density can be incorporated in a straightforward way by simply rejecting all trial SEDs that are incompatible with the upper limits.

3.2. *Trials on Galaxies of Known Redshifts*

To test the robustness of our SED template, we apply this photometric redshift technique to several well-studied submillimeter galaxies, and these results are summarized in Table 2. Disregarding the formal uncertainties for the moment, the new photometric redshifts z_{ph} are in excellent agreement with the spectroscopic redshifts z_{sp} for the all five submillimeter galaxies with known redshifts. When compared to the old radio-to-submillimeter spectral index estimates z_{SI} as shown in Figure 4, the improvement is seen mainly at high redshift ($z > 2$), where the effectiveness of the spectral index method diminishes because of the flattening of the α-z relation. Some improvement is generally expected for the new photometric method since more information is utilized. At the same time, this comparison also highlights the efficiency of the spectral index technique, which utilizes a rather limited amount of information.

The best-fit models are shown in Figure 5 for the four cases for which the most SED data exist. For the two well-studied SCUBA sources SMM J02399$-$0136 ($z = 2.80$; Ivison et al. 1998) and SMM J14011+0252 ($z = 2.57$; Ivison et al. 2000), we derive photometric redshifts of 2.83 and 2.73, respectively. The agreement with their spectroscopic redshifts is good in both cases, and the improvement over the α-z estimate is quite substantial for SMM J02399$-$0136. The excellent agreement in SMM J02399$-$0136 is somewhat fortuitous since the 1.4 GHz measurement is well above the

TABLE 2
REDSHIFT ESTIMATES FOR SUBMILLIMETER SOURCES

Name	z_{sp}	z_{SI}	z_{ph}	SFR[a]	N_{tot} (N_{det})[b]	χ_n^2[c]	References
Known redshifts:							
CUDSS 14.18....................	0.66	$1.12^{+0.53}_{-0.45}$	1.11 ± 0.21	200	5 (3)	0.02	1
SMM J02399−0134...........	1.06	$1.17^{+0.53}_{-0.45}$	0.93 ± 0.19	525	5 (3)	0.5	2
HR 10	1.44	$1.49^{+0.75}_{-0.53}$	1.75 ± 0.28	380	7 (5)	0.7	3,4,5
SMM J14011 + 0252..........	2.57	$2.53^{+1.24}_{-0.82}$	2.73 ± 0.37	850	5 (4)	1.0	2,6
SMM J02399−0136...........	2.80	$1.65^{+0.80}_{-0.53}$	2.83 ± 0.38	1400	9 (5)	28	2,7
No known redshifts:							
FIRBACK J1608 + 5418 ...	...	$0.05^{+0.21}_{-0.05}$	0.84 ± 0.18	690	7 (5)	17	12,13,14
SMM J14009 + 0252..........	...	$1.27^{+0.59}_{-0.54}$	1.30 ± 0.23	980	5 (4)	2.3	2,6
CUDSS 14.1....................	...	$2.01^{+1.10}_{-0.71}$	2.06 ± 0.31	520	7 (4)	0.5	10,11
Lockman 850.1.................	...	$2.95^{+1.49}_{-0.98}$	2.72 ± 0.37	570	8 (5)	0.2	15
SMM J00266 + 1708.........	...	$3.49^{+2.03}_{-1.23}$	3.50 ± 0.45	1200	6 (4)	0.2	2
SMM J09429 + 4658..........	...	≥ 3.6	3.86 ± 0.49	890	4 (4)	4.0	2,6
HDF 850.1	...	> 2.6	4.11 ± 0.51	380	8 (4)	0.8	8,9
QSOs:							
FSC 10214 + 4724.............	2.28	$1.49^{+0.74}_{-0.51}$	1.51 ± 0.25	2600	9 (9)	7.6	16,17
H1413 + 117	2.56	$0.88^{+0.41}_{-0.34}$	0.31 ± 0.13	850	9 (9)	28	17,18
LBQS 1230 + 1627.............	2.74	$2.19^{+1.16}_{-0.75}$	2.66 ± 0.37	1300	4 (4)	0.5	19,20,21
SMM J04135 + 1027..........	2.83	≥ 0.9	1.83 ± 0.28	1560	4 (3)	0.8	22
APM 08279 + 5255	3.87	$2.18^{+1.10}_{-0.71}$	1.74 ± 0.28	4900	7 (7)	9.4	23,24,25
BR 1335−0417	4.40	$1.81^{+0.95}_{-0.62}$	2.84 ± 0.38	1200	5 (5)	7.0	17,19,20,21,26
BR 0952−0115	4.43	$1.35^{+0.63}_{-0.46}$	0.96 ± 0.20	460	5 (4)	5.6	19,20,21,26
BR 1202−0725	4.70	$3.13^{+1.81}_{-1.14}$	3.20 ± 0.42	2300	11 (9)	3.1	17,19,20,21,26

[a] SFR is in $M_\odot$ yr^{-1}.

[b] N_{tot} and N_{det} are the total number of SED data used for the fit and the number of detections (i.e., $N_{tot} = N_{det} + N_{limits}$).

[c] $\chi_n^2 \equiv \chi^2/N_{det}$.

REFERENCES.—(1) Eales et al. 2000. (2) Smail et al. 2000. (3) Cimatti et al. 1998. (4) Dey et al. 1999. (5) Andreani et al. 2000. (6) Ivison et al. 2000. (7) Ivison et al. 1998. (8) Hughes et al. 1998. (9) Downes et al. 1999a. (10) Eales et al. 2000. (11) Gear et al. 2000. (12) Benford 1999. (13) Scott et al. 2000. (14) Dole et al. 2001. (15) Lutz et al. 2001. (16) Rowan-Robinson et al. 1993. (17) Benford et al. 1999. (18) Barvainis, Antonucci, & Coleman 1992. (19) Omont et al. 1996. (20) Guilloteau et al. 1999. (21) Yun et al. 2000. (22) Knudsen, van der Werf, & Jaffe 2001. (23) Irwin et al. 1998. (24) Lewis et al. 1998. (25) Downes et al. 1999b. (26) McMahon et al. 1999.
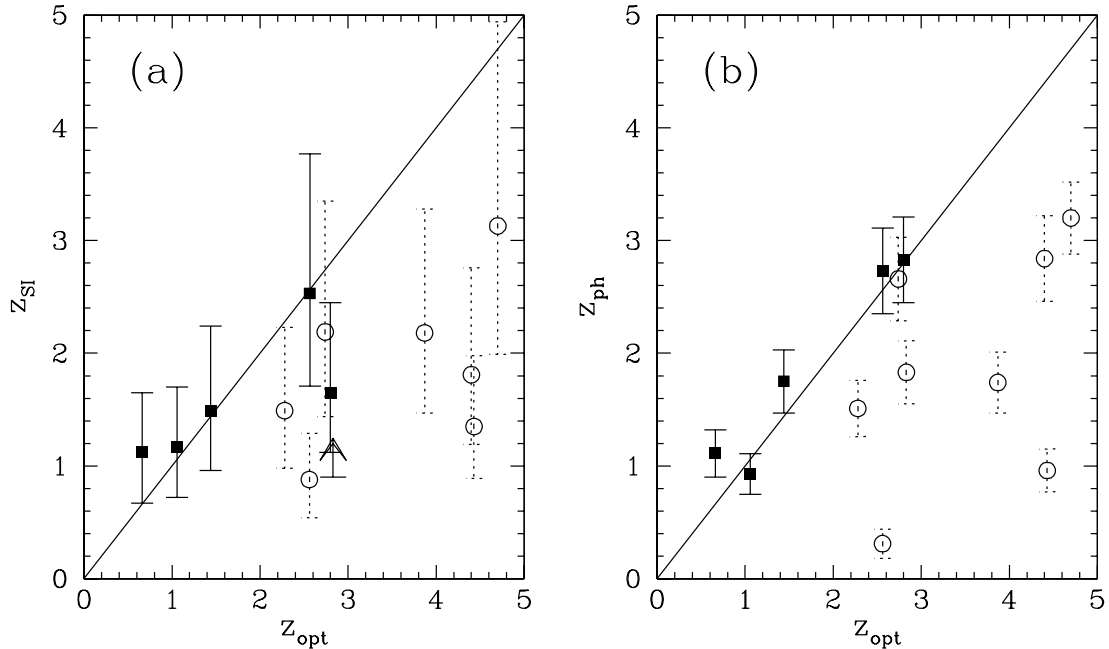

FIG. 4.—(a) Comparison plot of spectroscopic redshifts (z_{opt}) vs. redshift estimates from the radio-to-submillimeter spectral index (z_{SI}). (b) Comparison plot of spectroscopic redshifts (z_{opt}) vs. radio-to-FIR SED photometric redshifts (z_{ph}). Filled squares represent submillimeter galaxies, while the open circles are submillimeter-detected optical QSOs.
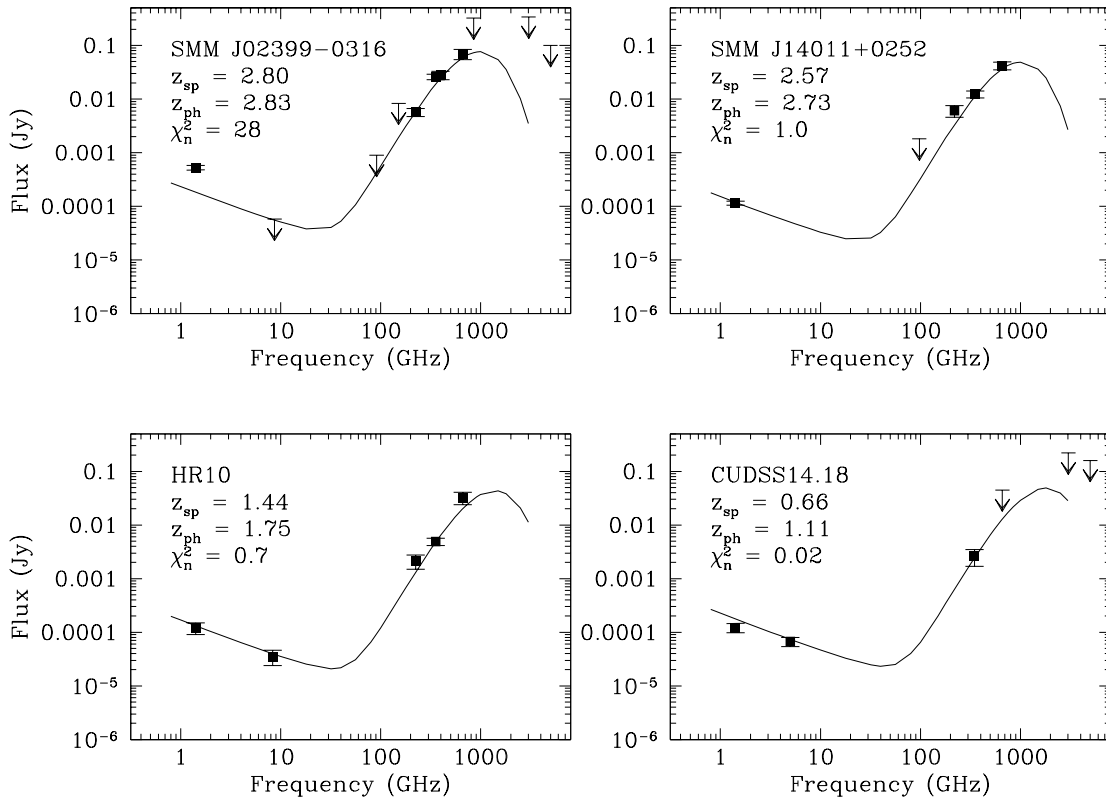
Fig. 5.—Results of the SED fits for four submillimeter galaxies with known spectroscopic redshifts

best-fit SED model (thus the source of a large reduced χ^2), but the best-fit solution is limited correctly by the 3 σ upper limit at 8.7 GHz. These two radio measurements are not consistent, and either the radio AGN is highly variable or the 1.4 GHz measurement may be affected by source confusion. The photometric redshifts (z_{ph}) for the submillimeter galaxies SMM J02399−0134 ($z = 1.06$; Smail et al. 2000) and HR 10 ($z = 1.44$; Cimatti et al. 1998; Dey et al. 1999) are also in good agreement with their spectroscopic redshifts within the uncertainty associated with the dust SED parameters (see § 4.4). The SED fit for HR 10 shown in Figure 5 suggests that the radio continuum is fainter than expected (i.e., $f_{nth} < 1$), which drove the z_{ph} to a slightly higher value. Only in CUDSS 14.18 ($z = 0.66$; Lilly et al. 1999) does the photometric redshift differ from the spectroscopic redshift by an amount larger than the nominal uncertainty of the technique. Only one submillimeter SED measurement exists for this galaxy, and this may be an important limiting factor. CUDSS 14.18 also appears to be slightly underluminous in radio continuum.

3.3. Photometric Redshifts for Submillimeter Galaxies

Since the great majority of the submillimeter galaxies are too faint to yield optical redshifts, a photometric technique may be the best way to infer their redshifts and evolution. We apply our photometric redshift technique to seven submillimeter galaxies whose spectroscopic redshifts are unknown but are suspected of being at high redshifts: HDF 850.1, Lockman 850.1, CUDSS 14.1, FIRBACK J1608+5418, SMM J00266+1708, SMM J09429+4658, and SMM J14009+0252. The photometric redshifts and

SFRs that we derive are summarized in Table 2, and the best-fit models for six cases are shown in Figure 6.

Perhaps the most interesting case is HDF 850.1, which is the brightest SCUBA source in the Hubble Deep Field (Hughes et al. 1998; Downes et al. 1999a). Despite the extraordinarily deep *Hubble Space Telescope* imaging data available, this submillimeter galaxy has eluded optical identification entirely. From the radio-to-submillimeter flux density ratio, we have previously estimated its redshift to be $z > 2.6$, but the flattening of the α-z relation at $z > 2$ meant that its redshift was not very well constrained (Carilli & Yun 1999). Our new photometric redshift analysis suggests that this galaxy has a high likelihood ($\chi_n^2 \sim 1$) of having a redshift near $z \sim 4.1$ with an intrinsic IR luminosity of about twice that of Arp 220. The uncertainty in the inferred redshift is too large ($\sigma_z \sim 0.5$) for a CO search using existing instruments, but a spectroscopic verification of HDF 850.1 and other optically faint submillimeter galaxies should become possible using future broadband instruments on the Green Bank Telescope or the Large Millimeter Telescope.

SMM J09429+4658 is another historically significant SCUBA galaxy, whose extremely dusty nature and red color ($K = 19.4$ mag, $I−K > 6$) was clearly demonstrated for the first time by the combined analysis of the high angular resolution VLA continuum imaging and deep near-IR imaging (Ivison et al. 2000). Our new photometric redshift analysis suggests a moderately high redshift ($z_{ph} \sim 3.9$), but the SED model fit (Fig. 6) is quite poor ($\chi_n^2 \sim 4$) since our SED template cannot be fully reconciled with the three existing SED measurements. One possible explanation is that this submillimeter galaxy is underluminous in radio continuum as in HR 10 and CUDSS 14.18 and its actual redshift is smaller.
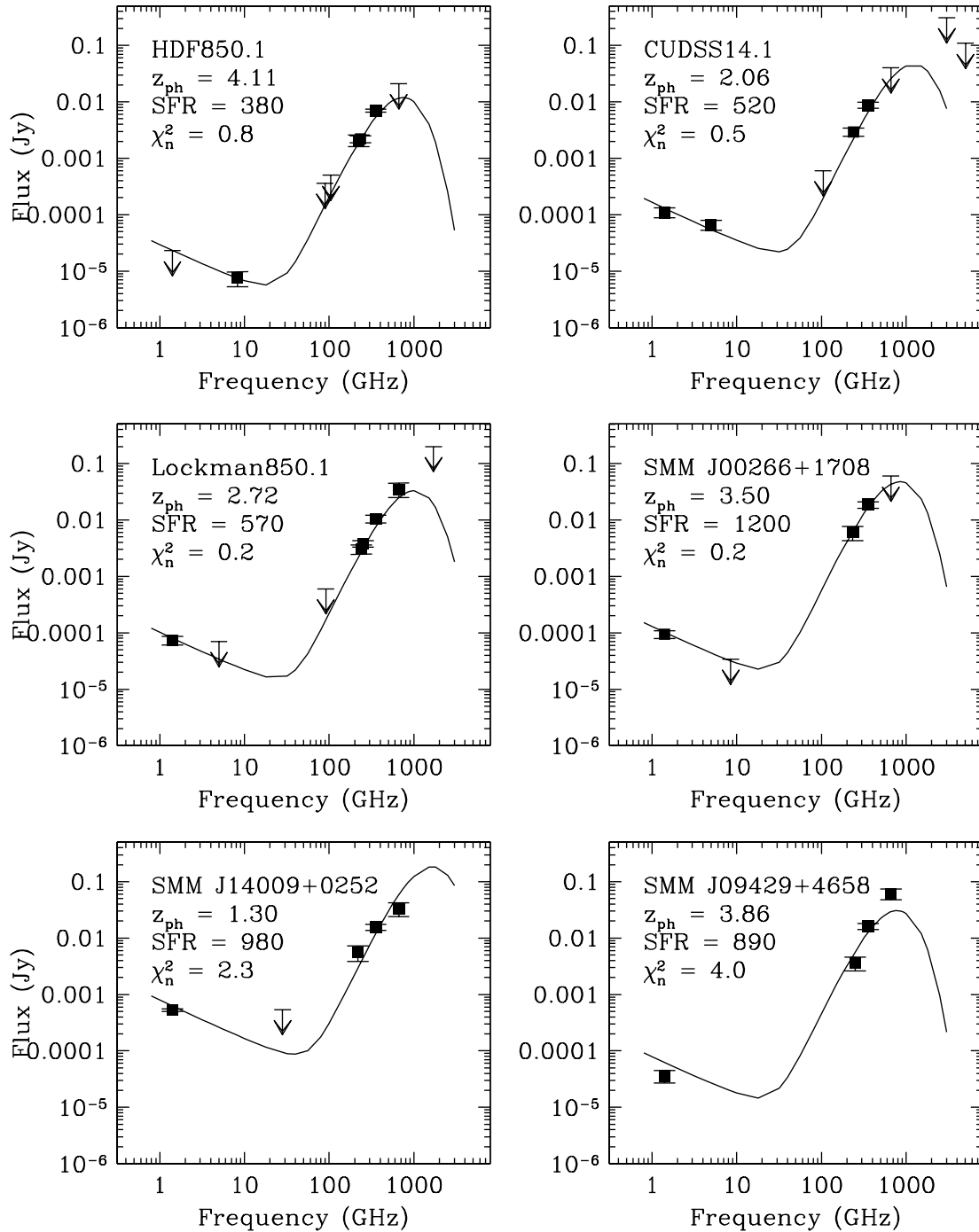
FIG. 6.—Results of the SED fits for six submillimeter galaxies with unknown redshifts are shown, including HDF 850.1

SMM J00266+1708 is another clear example of an optically faint ($K = 22.5$ mag) and red submillimeter galaxy, whose extreme properties are clearly established by the combined analysis of the high angular resolution millimeter continuum observations at the Owens Valley Radio Observatory and deep near-IR imaging using the Keck telescope (Frayer et al. 2000). The derived photometric redshift of $z_{ph} = 3.50$ makes it one of the highest redshift objects examined in this study, perhaps only the second after HDF 850.1, and it has the second-largest intrinsic FIR luminosity after SMM 02399−0136.

CUDSS 14.1 is the brightest SCUBA source discovered in the Canada France Redshift Survey 14 hr field by Eales et

al. (2000). Its optical counterpart has been identified using high angular resolution imaging at the VLA and IRAM interferometer (Eales et al. 2000; Gear et al. 2000), but it has not yet yielded a spectroscopic redshift. All four significant detection points lie along the model SED, while all upper limits are consistent with the model. The derived photometric redshift of $z_{ph} = 2.06$ is in good agreement with its optical photometric redshift of $z \sim 2$ (Lilly et al. 1999). Using the SED model of Dunne et al. (2000b) and optical–to–near-IR color, Gear et al. (2000) estimate its redshift to lie between 2 and 4.5.

Lockman 850.1 is the brightest SCUBA source detected in the Lockman Hole ISOPHOT survey region with an

extremely red ($K \sim 20$, $I–K > 6.2$) and extended optical counterpart (Lutz et al. 2001). Comparing the observed SED to that of Arp 220, Lutz et al. estimate its redshift to be around 3, which agrees well with our photometric redshift $z_{ph} = 2.72$.

SMM J14009+0252 is one of the submillimeter sources identified in the Abell 1835 field by Ivison et al. (2000) with a faint optical counterpart ($K \sim 21$). We derive $z_{ph} = 1.30$, but the SED fit shown in Figure 6 for the dust spectrum is poor ($\chi_n^2 = 2.3$). Ivison et al. rejected their own similarly modest redshift estimate because this galaxy is 3 times more luminous than HR 10 in the submillimeter while it is more than 10 times fainter in K. Its 1.4 GHz flux density is rather large for a SCUBA source, indicating a possible presence of a radio AGN. The SED fit for the dust spectrum alone suggests $z \sim 3.5$.

FIRBACK J1608+5418 is one of the FIR sources identified by the FIRBACK deep ISOPHOT survey (Dole et al. 2001). Incorporating its 350 and 450 μm detections at the Caltech Submillimeter Observatory and the VLA detection at 1.4 GHz, Benford (1999) estimated its redshift to be around $z \sim 1.5$. Our photometric redshift of $z_{ph} \sim 0.8$ is substantially smaller. Its radio-submillimeter flux density ratio suggests a presence of a radio AGN, and it is likely that higher than expected radio continuum flux density has led to a poor fit ($\chi_n^2 = 17$). Excluding the radio measurements, an SED analysis for the submillimeter/FIR dust peak alone suggests $z \sim 0.7$ with about 4 times larger FIR luminosity than Arp 220.

4. DISCUSSIONS AND SUMMARY

The above discussions of the SED modeling for the individual submillimeter detected galaxies clearly indicate that systematic SED variation among the individual galaxies is the dominant factor over the statistical uncertainty associated with the SED measurements. Here we discuss in detail the nature and the magnitude of the systematic effects associated with the dust and radio emission as well as the SED sampling and the intrinsic calibration uncertainties in the measurements. Their combined contribution to the photometric redshift uncertainty is quantified in § 4.4.

4.1. Effects of Dust Temperature and Emissivity

Doppler shift of a dust spectrum to a higher redshift is exactly equivalent to lowering of the dust temperature, and departure in T_d from the template SED translates directly to a redshift error (see Blain 1999 for further discussions). In other words, if the dust temperature of a galaxy is actually higher than our template, then the resulting z_{ph} would be an underestimate. While inherently subject to an object-to-object variation, the magnitude of uncertainty due to the spread in T_d is well understood quantitatively: $\Delta z \sim (\Delta T_d/T_d)(1 + z)$. If T_d is higher or lower by 10 K, the resulting error in the photometric redshift is about 0.3 at $z = 1$, and it grows as $(1 + z)$, reaching about 0.7 at $z = 3$.

Dust emissivity β is as important as dust temperature T_d because it determines the location of the low-frequency edge of the thermal dust feature in the SEDs. There is significant degeneracy between β and T_d (e.g., Dunne & Eales 2001), and the decoupling of the two becomes very difficult even when the dust spectrum is well sampled. In practice, only a few measurements along the rising part of the dust SED are

measured, and any deficiency in T_d is at least partly offset by the compensating effect of β. A trend supporting this effect is seen in Figure 2 as a broad trend of decreasing β with increasing T_d. A better demonstration of this effect is seen in Figure 1, where the submillimeter SED points alone might be fitted well by a dust spectrum with $T_d \sim 45$ K and $\beta \sim 1.5$. The observed trend of increasing T_d and deceasing β with increasing SFR is also clearly seen in the theoretical modeling of dust heating and emission using a self-consistent three-dimensional radiative transfer code by Misselt et al. (2001). Therefore, the error estimate based on the T_d alone might serve only as a reasonable upper bound.

4.2. Effects of the Radio Spectrum

Another reason why the photometric redshift error based on the scatter in T_d alone might be an overestimate is that our SED-fitting scheme relies as much on the spectral trough between the radio continuum and thermal dust emission as the dust spectrum itself. If this spectral trough is considered as the primary SED feature from which the photometric redshift information is derived, then it is easy to see that the variation in the dust spectrum is strongly modulated by the radio spectrum, which is not affected.

The radio spectrum has its own uncertainty in its overall scaling, as shown by the distribution of f_{nth} (see Fig. 3), and its contribution to the photometric redshift error has already been alluded to in § 3.2. The presence of a powerful radio AGN was a severe limiting factor for our earlier redshift estimation based on the radio-to-submillimeter spectral index (Carilli & Yun 1999), and it is not surprising that radio AGNs pose the biggest obstacle for the SED-fitting photometric technique as well. The photometric redshifts derived for an ensemble of QSOs that are associated with dusty hosts are given at the bottom of Table 2 (also see Fig. 4). Although there are exceptions such as LBQS 1230+1627 where $z_{ph} \sim z_{sp}$, the new photometric method does not fare much better than the spectral index method—the median $\chi_n^2 \sim 7$.

In practice, radio AGNs are not likely to limit the photometric redshift technique utilizing a starburst SED template because only a small minority of the known submillimeter galaxies show evidence of hosting a powerful AGN. Comparisons of deep X-ray and submillimeter surveys have shown very little overlap between the detected sources (e.g., Fabian et al. 2000; Hornschemeier et al. 2000; Barger et al. 2001). At least three out of five submillimeter galaxies discussed in § 3.2 are known to be AGN hosts, but the presence of an AGN also makes their spectroscopic redshift measurement possible and the use of a photometric technique unnecessary. The total fraction of infrared-selected galaxies whose radio-to-FIR SED shows a clear sign of an energetic AGN is only a few percent in the local universe (Yun et al. 2001), and this fraction appears to remain roughly the same at higher redshifts.

4.3. SED Sampling and Calibration

Another important source of uncertainty is poor sampling of the SED. Sampling only the radio part of the SED offers virtually no redshift information, and the same is true if only the submillimeter part of the SED is measured. On the other hand, because we are fitting the SED features changing over logarithmic scales, only a few well-placed SED data points are needed to derived the redshifts (Carilli

& Yun 1999). More than one measurement on both sides of the SED trough is highly desirable for a successful photometric redshift determination.

A related problem is the calibration and the relative weighting of individual SED measurements. Measurement uncertainties found in the literature often do not fully account for the overall calibration accuracy, as demonstrated by the magnitude of the scatter and the sizes of the error bars plotted for the SED measurements of Arp 220 in Figure 1. For example, the *IRAS* 60 and 100 μm measurements found in the Point Source Catalog (PSC) and the Faint Source Catalog (FSC) are known to have systemic calibration differences of order 10%, while the flux densities reported in the FSC often include uncertainties of only a few percent. For deriving the SED template from the 23 infrared selected starbursts, we adopted flux densities in the FSC but increased measurement uncertainties to 10% (unless the reported uncertainty was larger). This recalibration of the measurement uncertainty is more than cosmetic since the relative weights of the data points are directly reflected in the χ^2 minimization. We found this reweighting to be critically important in utilizing the submillimeter measurements. Similarly, all radio continuum measurements are assigned at least 10% uncertainty in order to account for the overall uncertainty in the flux calibration. No effort was made to recalibrate any of the submillimeter data points since most measurements generally carry relatively large fractional uncertainties, but some are clearly underestimates based on the SED plots such as shown in Figure 1. The same problems also plague the reported SED measurements of many submillimeter galaxies, and they will inevitably impact the accuracy of the photometric redshifts derived from these data. One way to improve the situation in the future would be to employ a frequency-selective bolometer (e.g., Kowitt et al. 1996; S. S. Meyer, D. Cottingham, T. C. Crawford, D. J. Fixsen, A. Goldin, M. S. Kowitt, J. Van Howe, & G. W. Wilson 2002, in preparation) that can make simultaneous measurements of several submillimeter bands with accurate relative calibration between the measurement bands.

4.4. *Estimate of Uncertainty in the Radio-to-FIR SED Technique*

The uncertainty of $\sigma_z \sim 0.3(1 + z)$ derived from the scatter in dust temperature is probably the upper bound to the error one might expect from the photometric technique using the dusty starburst SED template. The compensating effects of the dust emissivity and the radio continuum are more difficult to quantify as are the uncertainties contributed by the scatter in $f_{\rm nth}$. One way to estimate the collective uncertainty of the SED photometric technique is to apply this technique to the same 23 dusty starburst galaxies from which the SED template was derived. This is not entirely circuitous since our SED template is based only on the average properties of these galaxies and has no knowledge of dispersions. At the least, we may be able to confirm the impact of the 10 K scatter in the dust temperature on the dispersion in $z_{\rm ph}$ if dust temperature variation dominates the uncertainty in determining photometric redshifts.

The resulting "photometric redshift" $z_{\rm ph}$ for the 23 dusty starburst galaxies are listed in the last column of Table 1. There are several galaxies with negative $z_{\rm ph}$ since the impact of higher dust temperature for a $z = 0$ galaxy with $T_d > 58$
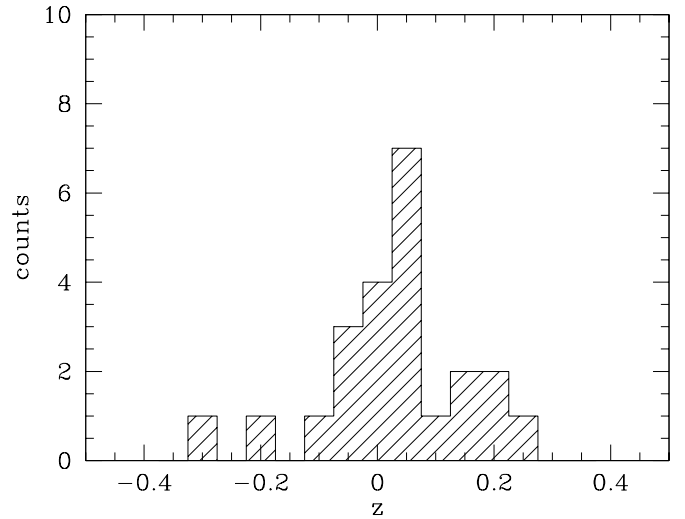

Fig. 7.—Histogram of "redshifts" for the 23 luminous infrared starbursts derived using our SED template.

K would result in $z_{\rm ph} < 0$. The χ^2 minimization program is modified to search a redshift range of $-1 \geq z_{\rm ph} \geq +1$ with modified scaling along the flux density axis in order to remove the nonphysical impact of negative redshift on D_L. A handful of galaxies with negative redshift are known (e.g., M81), but negative redshift is generally considered nonphysical. Here, the only physically meaningful interpretation of a negative $z_{\rm ph}$ that we derive is the measure of the magnitude of departure in the radio and dust property from the template SED, just the same way any uncertainty in $z_{\rm ph}$ should be interpreted at any redshift.

A histogram of the resulting photometric redshifts shown in Figure 7 suggests that the median "redshift" is about +0.05, suggesting the template SED may be slightly biased, but this offset is probably not very significant given the range of "redshifts" derived. "Photometric redshifts" as large as +0.3 and as small as −0.3 are found as expected from the scatter in T_d. The two extreme negative "$z_{\rm ph}$" objects IRAS 08572+3915 and Mrk 231 have T_d of 74 and 72 K, respectively, following the general trend expected of the dust temperature variation. On the other hand, two other dusty starburst galaxies with characteristic $T_d \geq 70$ K, IRAS 15250+3609 and IRAS 05189−2524, have "$z_{\rm ph}$" of +0.01 and +0.05, clearly demonstrating that there are other compensating effects and that the scatter in T_d alone does not dictate the overall photometric redshift uncertainty.

Regardless of the underlying causes, the "photometric redshifts" for two-thirds of all galaxies lie within $\Delta z \leq 0.10$, and we estimate that the collective uncertainty of the photometric redshift technique, including the variations in the radio and dust properties as well as the uncertainties in the χ^2 minimization process, is about 0.1 as long as this technique is applied to luminous dusty starburst galaxies only. Allowing for the $1 + z$ frequency folding of the Doppler effect, we estimate an overall uncertainty of $\sigma_z \sim 0.1(1 + z)$ with an upper bound in redshift uncertainty of about $0.3(1 + z)$.

In either case, this photometric redshift technique utilizing the radio-to-FIR dusty starburst SED represents a sig-

nificant step forward, particularly at high redshifts, when compared with existing methods. The full potential of this method will be realized when the sources identified by several large, deep, multifrequency surveys planned in the immediate future (e.g. *SIRTF* Legacy surveys) are analyzed together to reveal an accurate redshift distribution of luminous dusty galaxies at high redshift.

REFERENCES

Andreani, P., Cimatti, A., Loinard, L., & Rottgering, H. 2000, A&A, 354, L1
Barger, A., Cowie, L. L., & Richards, E. A. 2000, AJ, 119, 2092
Barger, A. J., Cowie, L. L., Steffen, A. T., Hornschemeier, A. E., Brandt, W. N., & Garmire, G. P. 2001, ApJ, 560, L23
Barger, A. J., et al. 1998, Nature, 394, 248
Barvainis, R., Antonucci, R., & Coleman, P. 1992, ApJ, 399, L19
Bell, A. R. 1978, MNRAS, 182, 443
Benford, D. J. 1999, Ph.D. thesis, Caltech
Benford, D. J., Cox, P., Omont, A., Phillips, T. G., & McMahon, R. G. 1999, ApJ, 518, L65
Blain, A. 1999, MNRAS, 309, 955
Blain, A., Smail, I., Ivison, R. J., & Kneib, J.-P. 1999, MNRAS, 302, 632
Carico, D. P., Keene, J., Soifer, B. T., & Neugebauer, G. 1992, PASP, 104, 1086
Carilli, C. L., & Yun, M. S. 1999, ApJ, 513, L13
———. 2000, ApJ, 530, 618
Chapman, S. C., et al. 2000, MNRAS, 319, 318
Cimatti, A., Andreani, P., Rottgering, H., & Tilanus, R. 1998, Nature, 392, 895
Condon, J. J. 1992, ARA&A, 30, 575
Condon, J. J., et al. 1998, AJ, 115, 1693
Condon, J. J., Huang, Z. P., Yin, Q. F., & Thuan, T. X. 1991, ApJ, 378, 65
Dey, A., Graham, J. R., Ivison, R. J., Smail, I., Wright, G. S., & Liu, M. C. 1999, ApJ, 519, 610
Dole, H., et al. 2001, A&A, 372, 364
Downes, D., et al. 1999a, A&A, 347, 809
Downes, D., Neri, R., Wiklind, T., Wilner, D. J., & Shaver, P. A. 1999b, ApJ, 513, L1
Downes, D., & Solomon, P. M. 1998, ApJ, 507, 615
Dunne, L., Clements, D. L., & Eales, S. A. 2000a, MNRAS, 319, 813
Dunne, L., & Eales, S. A. 2001, MNRAS, 327, 697
Dunne, L., Eales, S. A., Edmunds, M. G., Ivison, R. J., Alexander, P., & Clements, D. L. 2000b, MNRAS, 315, 115
Eales, S., et al. 1999, ApJ, 515, 518
Eales, S., Lilly, S., Webb, T., Dunne, L., Gear, W., Clements, D., & Yun, M. 2000, AJ, 120, 2244
Eales, S. A., Wynn-Williams, C. G., & Duncan, W. D. 1989, ApJ, 339, 859
Fabian, A. C., et al. 2000, MNRAS, 315, L8
Fox, M. J., et al. 2002, MNRAS, in press
Frayer, D. T., Ivison, R. J., Smail, I., Yun, M. S., & Armus, L. 1999, AJ, 118, 139
Frayer, D. T., Smail, I., Ivison, R. J., & Scoville, N. Z. 2000, AJ, 120, 1668
Gear, W. K., Lilly, S. J., Stevens, J. A., Clements, D. L., Webb, T. M., Eales, S. A., & Dunne, L. 2000, MNRAS, 316, L51
Guiderdoni, B., Hivon, E., Bouchet, F. R., & Maffei, B. 1998, MNRAS, 295, 877
Guilloteau, S., Omont, A., Cox, P., McMahon, R. G., & Petitjen, P. 1999, A&A, 349, 363

Hildebrand, R. H. 1983, QJRAS, 24, 267
Hines, D. C., & Low, F. J. 1999, in ASP Conf. Ser. 191, Photometric Redshifts and the Detection of High Redshift Galaxies, ed. R. Weymann, L. Storrie-Lombardi, M. Sawicki, & R. Brunner (San Francisco: ASP), 265
Hornschemeier, A. E., et al. 2000, ApJ, 541, 49
Hughes, D. H., et al. 1998, Nature, 394, 241
Irwin, M. J., Ibata, R. A., Lewis, G. F., & Totten, E. J. 1998, ApJ, 505, 529
Ivison, R. J., et al. 1998, MNRAS, 298, 583
———. 2000, MNRAS, 315, 209
Kennicutt, R. C. 1998, ApJ, 498, 541
Knudsen, K. K., van der Werf, P. P., & Jaffe, W. 2001, in Deep Millimeter Surveys: Implications for Galaxy Formation and Evolution, ed. J. D. Lowenthal & D. H. Hughes (Singapore: World Scientific), 168
Kowitt, M. S., Fixsen, D. J., Goldin, A., & Meyer, S. S. 1996, Appl. Opt., 35, 5630
Lewis, G. F., Chapman, S. C., Ibata, R. A., Irwin, M. J., & Totten, E. J. 1998, ApJ, 505, L1
Lilly, S. J., et al. 1999, ApJ, 518, 641
Lisenfeld, U., Isaak, K. G., & Hills, R. 2000, MNRAS, 312, 433
Lutz, D., et al. 2001, A&A, 378, 70
Matsuhara, H., et al. 2000, A&A, 361, 407
McMahon, R. G., Priddey, R. S., Omont, A., Snellen, I., & Withington, S. 1999, MNRAS, 309, L1
Misselt, K. A., Gordon, K. D., Clayton, G. C., & Wolff, M. J. 2001, ApJ, 551, 277
Omont, A., et al. 1996, A&A, 315, 1
Rigopoulou, D., Lawrence, A., & Rowan-Robinson, M. 1996, MNRAS, 278, 1049
Rowan-Robinson, M., et al. 1993, MNRAS, 261, 513
Sakamoto, K., Scoville, N. Z., Yun, M. S., Crosas, M., Genzel, R., & Tacconi, L. J. 1999, ApJ, 514, 68
Scott, D., et al. 2000, A&A, 357, L5
Scott, S. E., et al. 2002, MNRAS, in press
Scoville, N. Z., Sargent, A. I., Sanders, D. B., & Soifer, B. T. 1991, ApJ, 366, L5
Scoville, N. Z., Yun, M. S., & Bryant, P. M. 1997, ApJ, 484, 702
Smail, I., et al. 1999, MNRAS, 308, 1061
Smail, I., Ivison, R., & Blain, A. 1997, ApJ, 490, L5
Smail, I., Ivison, R. J., Owen, F. N., Blain, A. W., & Kneib, J.-P. 2000, ApJ, 528, 612
Solomon, P. M., Downes, D., Radford, S. J. E., & Barrett, J. W. 1997, ApJ, 478, 144
Steidel, C. C., Adelberger, K. L., Giavalisco, M., Dickinson, M., & Pettini, M. 1999, ApJ, 519, 1
Yun, M. S., et al. 2000, ApJ, 528, 171
Yun, M. S., Reddy, N., & Condon, J. 2001, ApJ, 554, 803
Yun, M. S., & Scoville, N. Z. 1998, ApJ, 507, 774